A simple strategy for synthesizing highly luminescent carbon nanodots and application as effective down-shifting layers

2015 Nanotechnology 26 065402

(http://iopscience.iop.org/0957-4484/26/6/065402)

IOP Publishing Nanotechnology
Nanotechnology **26** (2015) 065402 (11pp) doi:10.1088/0957-4484/26/6/065402

A simple strategy for synthesizing highly luminescent carbon nanodots and application as effective down-shifting layers

Xugen Han[1], Sihua Zhong[1], Wei Pan[1] and Wenzhong Shen[1,2]

[1] Laboratory of Condensed Matter Spectroscopy and Opto-Electronic Physics, and Key Laboratory of Artificial Structures and Quantum Control (Ministry of Education), Department of Physics and Astronomy, and Institute of Solar Energy, Shanghai Jiao Tong University, Shanghai 200240, People's Republic of China
[2] Collaborative Innovation Center of Advanced Microstructures, Nanjing University, Nanjing, 210093, People's Republic of China

E-mail: wzshen@sjtu.edu.cn

Received 4 December 2014, revised 20 December 2014
Accepted for publication 2 January 2015
Published 22 January 2015

Abstract

We propose a novel strategy to prepare highly luminescent carbon nanodots (C-dots) by employing a hydrothermal method with citric acid as the carbon source and ethylenediamine as the nitrogen source, together with adding moderate ammonia water (AW) to achieve both appropriate inner structure and excellent N passivation. The effect of pH value and AW amount on the luminescence properties has been thoroughly investigated. The photoluminescence quantum yield of the resultant C-dots reaches as high as 84.8%, which is of 10.56% higher than that of the C-dots synthesized in the absence of AW in the reaction precursors. We have further combined the highest luminescent C-dots with polyvinyl alcohol to form luminescent down-shifting layers on silicon nanowire solar cells. An effective enhancement of short-circuit current density has been realized and the contribution of the down-shifting has been extracted quantitatively from the deterioration of surface reflectance and the gain of the optical absorption redistribution by means of a theoretical model on external quantum efficiency analysis.

S Online supplementary data available from stacks.iop.org/NANO/26/065402/mmedia

Keywords: carbon nanodots, high luminescence, down-shifting, ammonia water, silicon nanowire solar cells

(Some figures may appear in colour only in the online journal)

1. Introduction

During the past decade, luminescent down-shifting (LDS) functional materials, such as rare earth ions [1–3], II–VI semiconductor quantum dots (QDs) [4–7] and organic dyes [8–11], have attracted considerable attention due to their distinct large Stokes shifts that have been widely used on optoelectronic devices. However, those LDS materials are limited by their inherent deficiency, such as narrow absorption band, high toxicity and poor photostability for rare earth ions (like Eu^{3+}) [1], semiconductor QDs (like CdS) [6] and organic dyes [12], respectively. It is thus of paramount importance to develop other luminescent materials with high performance and low environmental hazard. In recent years, fluorescent carbon nanomaterials, especially carbon nanodots (C-dots) and graphene QDs, have been widely investigated and applied to bioimaging and sensing because of their outstanding optical properties, low toxicity, excellent biocompatibility and abundance of raw material in nature [13–21]. Compared with graphene QDs, luminescent C-dots, consisting of numerous functional groups on their surface, usually possess higher photoluminescence quantum yield (PLQY) and are particularly encouraging as an alternative.

However, the PLQY of early-stage luminescent C-dots was less than 20% [14, 22], far lower than that of the commonly used LDS materials of more than 50% [3, 4]. Surface passivation has been the key technique to enhance the PLQY of luminescent C-dots [14, 20, 23]. It has been reported that high PLQY of luminescent C-dots could be achieved by modifying their surface states with different surface-passive agents, such as *N*-(*β*-aminoethyl)-*γ*-aminopropyl methyldimethoxy silane (PLQY reaches 47%) [20], 1-hexadecylamine (53%) [14] and PEG_{1500N} together with TiO_2 (70%) or ZnS (78%) after a gel column fractionation [24]. Nevertheless, the fabrications of C-dots treated by these materials often have some drawbacks, such as rigorous conditions, high temperature and time-consuming processes, which restrict their applications. The control of inner structure by atomic doping, especially N doping, has shown the potential for widespread adoption due to its efficient one-step strategy, numerously alternative compounds and large-scale fabrication [18, 25], although the exact mechanism of the high luminescence is still unclear. Zhou *et al* [13], and Guo *et al* [26], have synthesized N-doped C-dots by carbonizing sodium citrate at 180 °C in the presence of urea and ammonium bicarbonate as N-doping sources to realize the PLQY of 42% and 68%, respectively. Zhu *et al* [19], and Dong *et al* [27], have employed citric acid (CA) as the carbon source to demonstrate PLQY as high as 80% and 73% with ethylenediamine (EDA) and L-cysteine as the atom-doping agents, respectively.

In this work, we report on a new strategy for yielding highly luminescent C-dots. On the basis of successful realization of PLQY of 76.7% C-dots with CA as the carbon source and EDA as the nitrogen source, we propose for the first time ammonia water (AW) as both the surface passivator and the inner structure modifier to boost the PLQY of C-dots up to 84.8%. The keys lie in the fact that AW can effectively passivate the surface of C-dots through substituting amide groups for carboxyl groups, and modify the inner structure of C-dots by eliminating oxygen state. We have further combined the highest luminescent C-dots with polyvinyl alcohol (PVA) to form LDS layers on silicon nanowire (SiNW) solar cells. A theoretical model on the external quantum efficiency (EQE) analysis has also been set up to quantitatively measure the contribution of down-shifting from the observed enhancement in short-circuit current density (J_{SC}).

2. Experimental section

2.1. C-dots synthesis

The C-dots were synthesized by using a hydrothermal method. In brief, 0.787 g CA, 251 μL EDA and various amount of AW (including 0 M, i.e. without AW) were mixed in 10 mL deionized water (DI-water), and then the reaction precursors were transferred to a 30 mL Teflon-lined autoclave and heated at 160 °C for 3 h. After quickly cooling the Teflon-lined autoclave to room temperature by water, the well-dispersed C-dots aqueous solutions were obtained. The C-dots were purified through a dialysis membrane (500 MWCO) for 24 h. Dialysis is used here mainly to remove the small molecules in the as-prepared C-dots solutions. All the products were treated by ultrasonic oscillation before further use and characterization.

2.2. SiNW solar cells and LDS layer fabrication

SiNW arrays (SiNWs) with a length of 400 nm were synthesized on one side of p-type (~2 Ω cm, 200 ± 20 μm) silicon (100) wafers using a two-step, metal-assisted chemical etching technique [28]. The SiNW solar cells were fabricated by a standard solar cell manufacturing process, and the finished solar cells were cut into $3 \times 3\ cm^2$ pieces to measure both electrical and optical characteristics. To successfully apply the resultant C-dots on the SiNW solar cells as an LDS layer, we used PVA as the host material for the LDS layer, based on its high transmittance and good compatibility with our C-dots. The yielded highest luminescent C-dots aqueous solutions were mixed with the PVA aqueous solutions (5 wt%) to obtain the C-dots/PVA solutions. Next, we spin-coated the C-dots/PVA solutions on the SiNW solar cells and heated at 80 °C for 20 mins to form the LDS layers, the thickness of which is adjusted by the spin-coating times.

2.3. Characterization

The morphologies of the C-dots were characterized by a JEOL (Japan) JEM-2100F transmission electron microscopy (TEM). The Raman spectrum of the C-dots was examined at room temperature by a Jobin Yvon (France) LabRam HR800 UV micro-Raman spectrometer using a He-Cd (325.0 nm) laser. The UV-visible (UV–Vis) spectra were measured by a Perkin-Elmer (USA) Lambda 20 spectrometer. The steady-state PL spectra and fluorescence lifetimes were recorded using a steady-state and time-resolved fluorescence spectrofluorometer (QM/TM/IM, PTI, USA). The x-ray photoelectron spectroscopy (XPS) spectra of the products were carried out with a Shimadzu (Japan) Kratos Axis Ultra DLD spectrometer using a monochromatic Al Kα x-ray source (1486.6 eV). The Fourier transform infrared spectroscopy (FTIR) spectra were taken with a Bruker (Germany) Vertex 70 spectrometer at room temperature from 400 to 4000 cm^{-1}. The samples, used for both the XPS and FTIR spectra measurements, were prepared by repeatedly dropping the purified C-dots solutions on silicon slices and then drying them in an oven. The morphologies of the SiNW solar cells were examined by a Philips (Netherlands) FEI Sirion 200 field emission scanning electron microscopy (SEM). Both the reflectance and the EQE spectra of the samples were performed in the 300–1100 nm wavelength range by a PV Measurements (USA) QEX10 system. The current–voltage characteristics of the SiNW solar cells coated with and without the LDS layer were measured at standard test conditions (an irradiation intensity of 1000 W m^{-2}, AM 1.5 G, and a temperature of 25 ± 0.5 °C) using a Newport (USA) Oriel Sol2A solar simulator with a Keithley 2400 source meter. Five current–voltage measurements were taken for

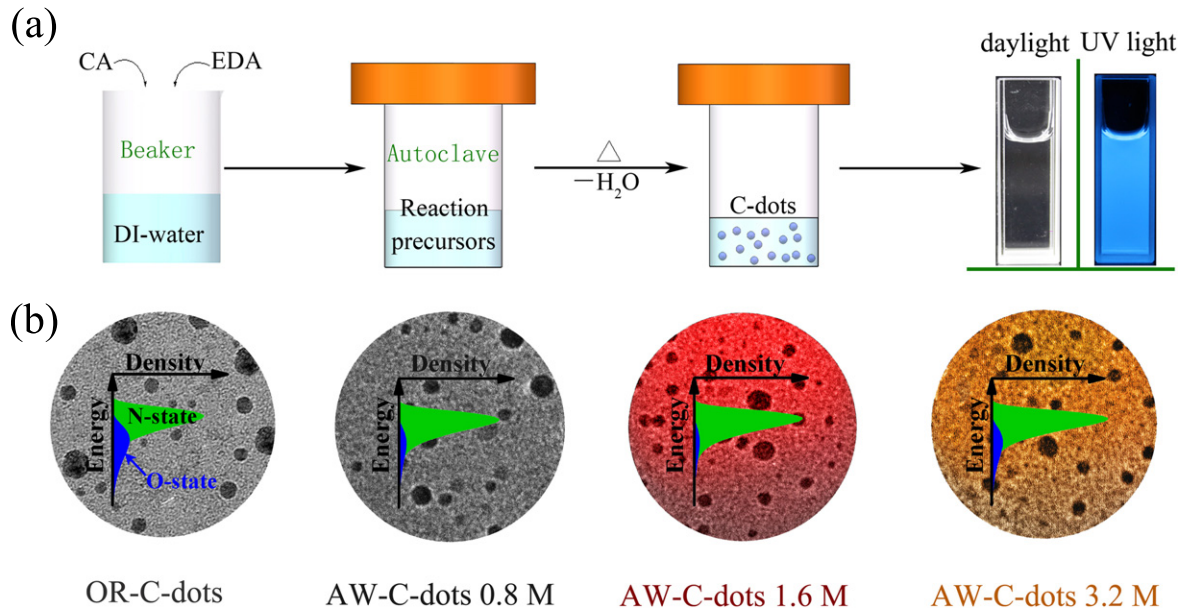

Figure 1. (a) Schematic diagram for the synthesis of C-dots. (b) Schematic diagram of different C-dots synthesized with 0, 0.8, 1.6 and 3.2 M ammonia water (AW) in the reaction precursors. The green area represents the N-state, and the blue one is O-state.

each case, and the standard deviation between measurements was lower than 0.03%.

3. Results and discussion

3.1. Characterization of C-dots

The luminescent C-dots were hydrothermally synthesized by using CA and EDA as reaction precursors. Figure 1(a) shows the schematic of the synthetic process. First, CA and EDA were mixed in DI-water, and then the mixture was transferred to a Teflon-lined autoclave and heated at 160 °C for 3 h to obtain the C-dots. The digital pictures of the C-dots aqueous solutions, displayed in figure 1(a), clearly show that the obtained C-dots exhibit bright blue fluorescence under the illumination of a 365 nm UV light lamp. Figure 2(a) shows the TEM image of the C-dots, revealing that the C-dots are well dispersed with an average diameter of 3.7 nm (ranging from 2 to 8 nm). The Raman spectrum has also been carried out to feature the characteristic bands of the C-dots to a certain extent, as shown in figure 2(b). It displays the G-band at 1597 cm^{-1} relevant to sp^2 carbon and the D-band at 1305 cm^{-1} relevant to sp^3 carbon [29], indicating that the C-dots are composed of sp^2 domain embedded in sp^3 matrix. We have carried out a detailed study on the UV–Vis absorption and PL spectra of the C-dots (figure 2(c)), which are of paramount importance for its application in optoelectronic devices as a down-shifting layer. The UV–vis spectrum evidently indicates that the C-dots mainly absorb the light in the wavelength below 400 nm with two characteristic absorption peaks. It is believed that the absorption peak at 239 nm originates from the $\pi \rightarrow \pi^*$ transition aromatic C=C bonds [17, 29], and that centered at 348 nm is from the trapping of excited-state energy by the surface N-state [27]. In the PL spectrum, a strong luminescence centered at 439 nm with a full width at half maximum of 70 nm is observed upon excitation of the C-dots aqueous solutions at 360 nm, demonstrating the feasibility of the C-dots as LDS materials. As shown in figure 2(d), its emission peak has no obvious shift as the excitation wavelength varies from 300 to 390 nm, and the PL intensity reaches the maximum at the excitation wavelength of 350 nm. This value is close to 348 nm absorption peak, demonstrating that the PL is related to the surface N-state.

3.2. The pH effect on the PL property of C-dots

In general, the luminescence and absorption features of molecular fluorescent materials can be influenced by pH. Here, we have further investigated the pH effect on the luminescence property of the resultant C-dots. The pH value of the above-yielded C-dots aqueous solutions is 5.64 and the pH conditions of the C-dots, used for the pH effect investigation, are regulated by sulfuric acid and sodium hydroxide. Figure 2(e) displays the absorption spectra of C-dots aqueous solutions with varied pH values of 1, 7 and 13, indicating that absorption peak at 348 nm remains stable in both strong base and neutral solutions, but redshifts to 366 nm when pH is 1. Similarly, it is found from figure 2(f) that the PL peak is fixed at 439 nm when the pH is higher than 4, and redshifts when the pH is lower than 4. Figure 2(f) also shows the pH-dependent integrated PL intensity, which remains almost constant in a solution of pH 4–10, but decreases quickly in the solution with a higher or lower pH value. This observation can also be confirmed by the digital photos of the C-dots aqueous solutions under the illumination of 365 nm UV light (inset of figure 2(f)), with much brighter color of the pH = 7 sample as compared with its pH = 1 and 13 counterparts. The effect of pH can be understood in terms of the change in the

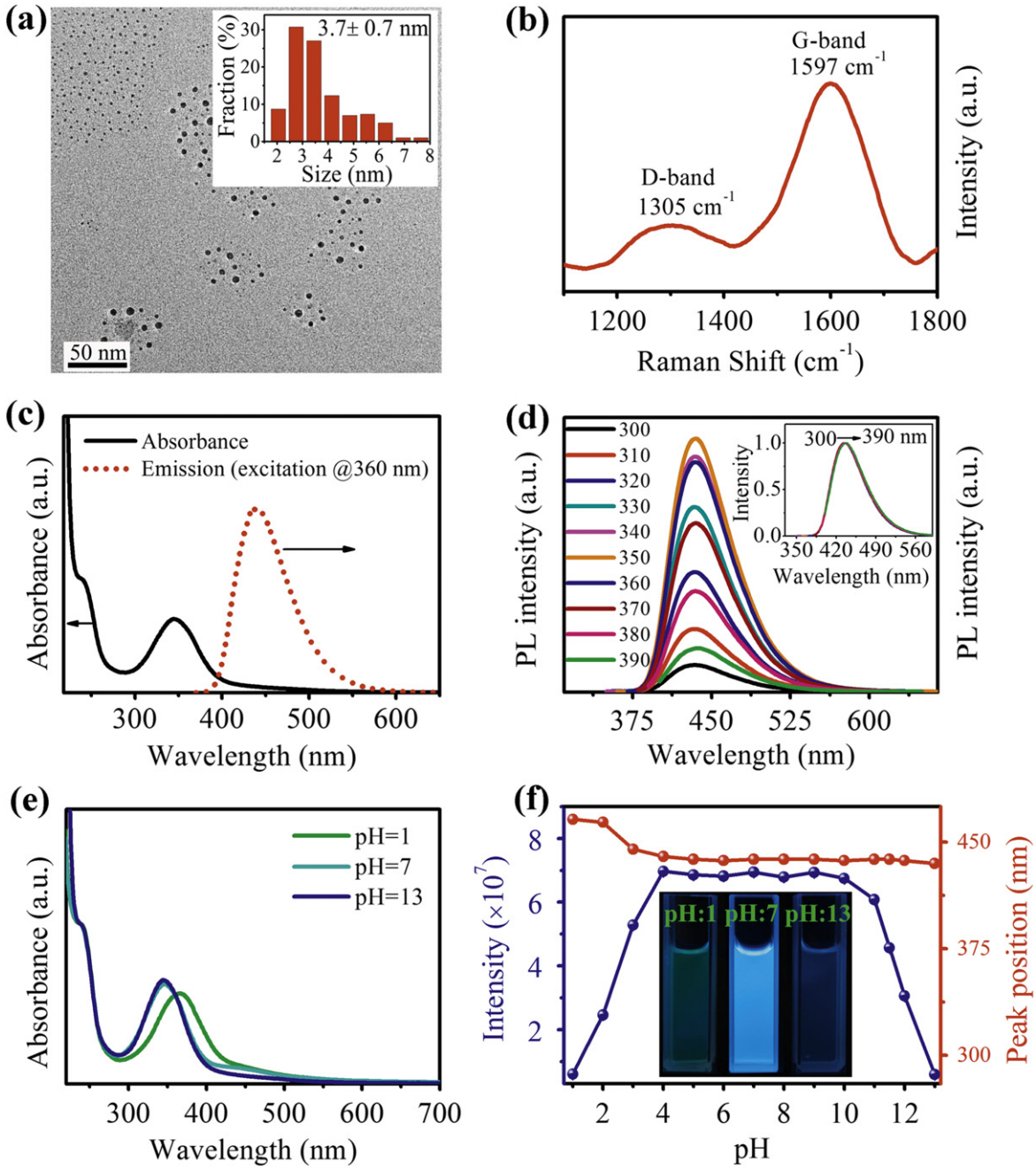

Figure 2. (a) TEM image of the C-dots. The inset shows the size distribution of the C-dots. (b) Raman spectrum of the C-dots. (c) UV–vis absorption (black solid curve) and PL (red dot curve) spectra excited at 360 nm of the C-dots aqueous solutions. (d) PL spectra of the C-dots excited by different wavelengths. The inset shows the corresponding normalized PL spectra. (e) Absorption spectra. (f) Effect of pH on the integrated PL intensity and the PL peak position of the OR-C-dots excited at 360 nm. Inset shows the digital photos of the OR-C-dots aqueous solutions illuminated by a 365 nm UV light lamp with the pH of 1, 7 and 13, respectively.

surface functional groups owing to protonation/deprotonation [26, 27].

3.3. Enhanced PL property of C-dots by AW

The PLQY is a widely used parameter for luminescent materials. Excitingly, the PLQY of the resultant C-dots is measured to be as high as 76.7% (excited at 360 nm) by using quinine sulfate as a reference (see details in table S1), which is similar to the result reported by Zhu *et al* [19], but much higher than most of the previous reports [13, 20, 30]. The high luminescence is probably related to the surface N-state, which has been mentioned previously in section 3.1. To prove this, we designed a control experiment to cap more N atoms on the OR-C-dots surface, by using a very reactive reagent, AW, to post-treat the resultant OR-C-dots at 100 °C for 1 h. The much lower heating temperature and shorter reaction time are controlled to avoid a change in the inner carbon backbone structure of the OR-C-dots. Through this simple process, the PLQY of the OR-C-dots is enhanced from 76.7% to 79.5%.

FTIR spectra in figure S1 illustrate that amide groups replaced the carboxyl groups capping on the surface of C-dots because of the enhancement of the C–N bond at 1232 cm^{-1} and the C=O bond (1655 cm^{-1}) due to the amide group, as well as the decrease of the C=O bond (1708 cm^{-1}) due to the carboxyl group. This surface treatment brought a 3.65% increase of PLQY, showing that the PL is related to the surface N-state induced by the amide groups.

Many research studies have pointed out that the fluorescence of carbon nanoparticles is related to the surface/edge state induced by the surface functional groups [31–35]. Recent literature about the PL in C-dots and graphene quantum dots [36] has illustrated that surface functional groups can combine with several edge carbon atoms in carbon backbone to form a molecule-like surface/edge state which contributes to the luminescence. A similar conclusion has reached from research on graphene oxide, which suggests that fluorescence comes from the recombination of electron-hole pairs localized in small sp^2 carbon domains surrounded by a carbon-oxygen sp^3 matrix [37]. Therefore, there is an expectation to obtain C-dots with a higher PLQY by effective surface passivation with amide groups and precise control of inner structure. To achieve this, we propose to add various amount of AW to the precursor after considering its 1) high reactivity [38] and 2) low viscosity (thus beneficial to practical application) [19]. For convenience, we name the C-dots synthesized with 0, 0.8, 1.6 and 3.2 M AW as OR-C-dots, AW-C-dots 0.8 M, AW-C-dots 1.6 M and AW-C-dots 3.2 M, respectively.

Figure 3(a) displays the PL spectra (excited at 360 nm) of OR-C-dots and AW-C-dots aqueous solutions, whose absorbance at 360 nm is controlled to be 0.03 by adjusting the concentration. From this figure, it is clear that AW did not change the emission wavelength, but the PL intensity and thus the PLQY. The inset of figure 3(a) displays the different color of C-dots synthesized with a different AW concentration. Figure 3(b) shows the variation of PLQY with AW concentration, which increases at first and then decreases with the increasing AW concentration. The PLQY reaches as high as 84.8% for the AW-C-dots 1.6 M—much higher than that of the OR-C-dots. The enhancement factor is 10.56%—higher than that of 3.65% resulted by post-treatment of OR-C-dots with AW, suggesting that AW brings an extra enhancement of PLQY induced by the change in inner structure.

To further explore the relationship between the PLQY and structure of C-dots, we employed XPS and FTIR techniques to reveal the chemical bonds and compositions in OR-C-dots and AW-C-dots. XPS spectra in figure 4(a) indicate that all the C-dots are mainly composed of carbon, nitrogen and oxygen, where two extra peaks Si_{2p} and Si_{2s} come from silicon substrate. The C_{1s} spectra in figure 4(b) demonstrate the existence of C=C (284.6 eV), C–N (286.0 eV), C–O (286.8 eV) and C=O (288.4 eV) [21]. The O_{1s} spectra in figure 4(c) display the presence of C=O (531.3 eV) and C–OH/C–O–C (532.4 eV) [16]. The N_{1s} spectra in figure 4(d) give the peaks of C–N–C (399.5 eV), N–$(C)_3$ (400.5 eV) and N–H (401.5 eV) [21, 39]. FTIR spectra in figure 4(e) also illustrate that these C-dots are composed of aromatic CN

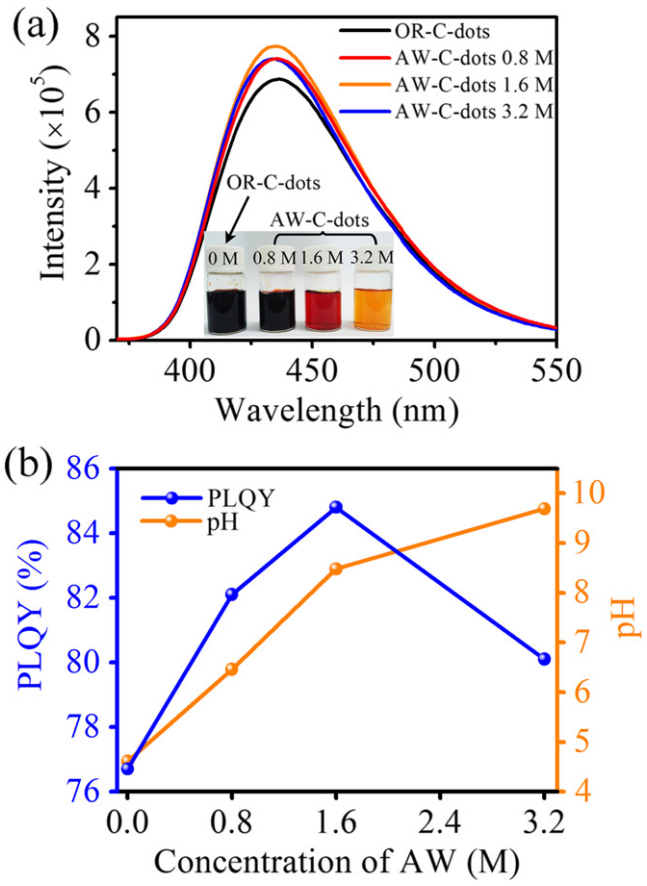

Figure 3. (a) PL spectra of OR-C-dots and AW-C-dots when excited at 360 nm. The inset shows their digital photos. (b) PLQY of the resultant C-dots and pH of the reaction precursors with different AW concentrations.

heterocycles [21] due to the existence of N–H (at 3187 cm^{-1}), C–H (2925 cm^{-1}), C–N (1232 cm^{-1}) stretching vibrations and N–H (at 1559 cm^{-1}), C–H (781 cm^{-1}) bending vibrations. Furthermore, from this figure, it is clear that compared to OR-C-dots, more amide groups are bonded to the surface of AW-C-dots because of the obvious weakening of C=O stretching vibration (1708 cm^{-1}) due to carboxyl groups and the increase of C=O peaks (1655 cm^{-1}) due to amide groups. The detailed XPS data in table 1 further indicate that the use of AW in the synthesis can increase the N–H bond, i.e., enhance the surface passivation by amide groups, which can finally increase the surface N-state. At the same time, AW has an obvious effect on O and C contents in C-dots. Moderate AW decreases the O content, which may decrease the O defect states in the C-dots, while excess AW has an opposite effect.

It is worth noting that PLQY does not increase with the increasing amide group (N–H bond). Actually, it increases with the decreasing O-state, or with the increasing ratio of N-state to O-state ($R_{N/O}$), as shown in figure S2. This implies that the key to enhancing PLQY is to enhance the N-state by excellent N-passivation and to remove the O-state in the N-doped C-dots by inner structure modification. A similar viewpoint has been proposed by Dong *et al* [27]. They have pointed out that a high PLQY and excitation-independent

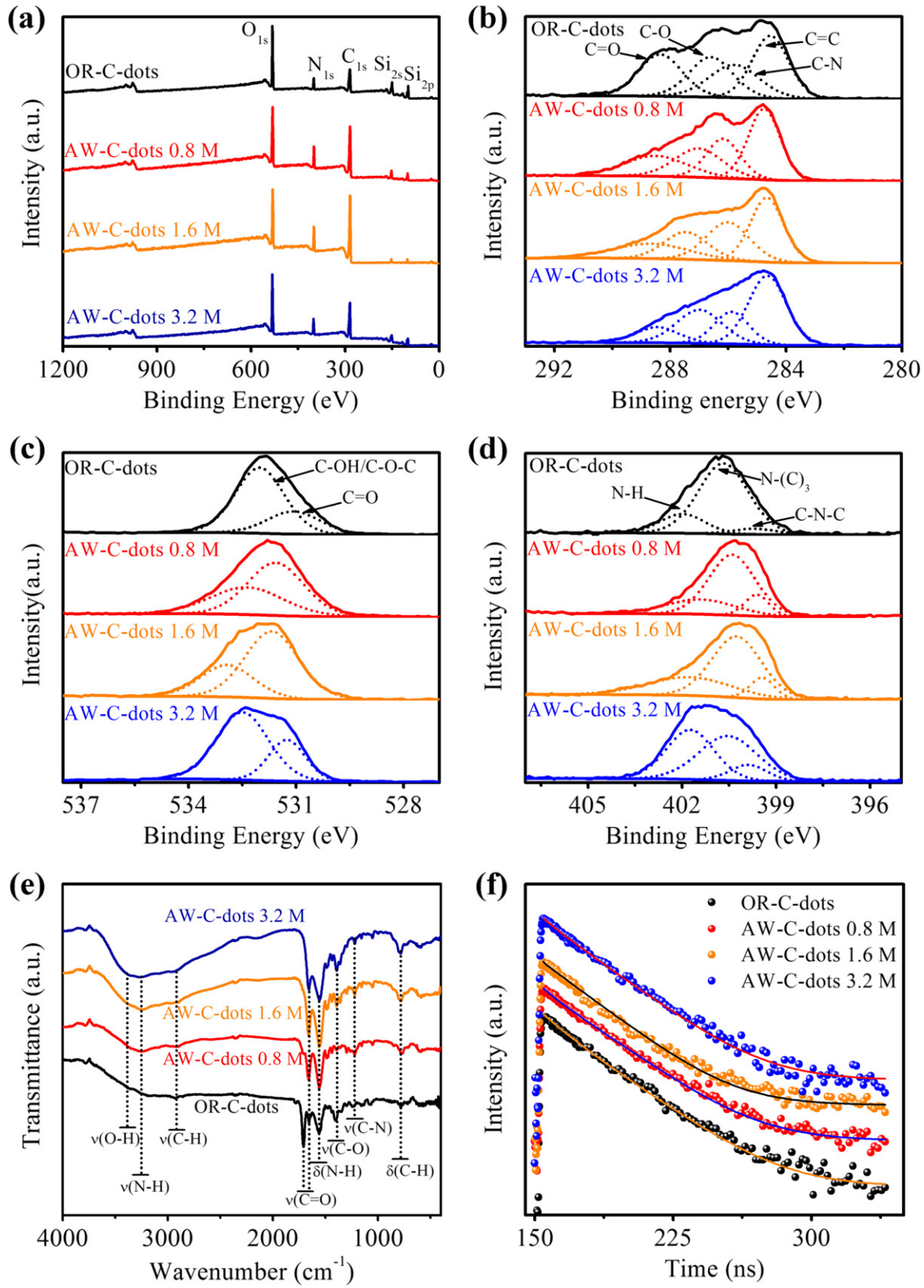

Figure 4. (a) XPS survey scan, (b) C_{1s} spectra, (c) O_{1s} spectra, (d) N_{1s} spectra, (e) FTIR spectra and (f) PL decay curves of OR-C-dots and AW-C-dots detected at 439 nm with the excitation of 350 nm.

Table 1. Atomic concentration and N bonds concentration of C-dots summarized from the XPS observation.

	Atomic concentration (%)[a]			N bonds concentration (%)		
Samples	C	O	N	N–H	N-$(C)_3$	C-N-C
OR-C-dots	55.56	32.72	11.72	18.57	75.85	5.57
AW-C-dots 0.8 M	67.21	20.64	12.15	23.65	64.50	11.86
AW-C-dots 1.6 M	69.89	17.97	12.13	30.09	59.68	10.23
AW-C-dots 3.2 M	61.61	26.61	11.77	42.59	46.64	10.77

[a] Hydrogen is not taken into account for the calculation of atomic concentration.

Table 2. Fitting parameters for the PL decay curves of the C-dots[a], together with their PLQY.

Samples	A_1 (%)	τ_1 (ns)	A_2 (%)	τ_2 (ns)	PLQY (%)
OR-C-dots	13.0	10.2	87.0	22.8	76.7
AW-C-dots 0.8 M	0.3	6.3	99.7	22.5	82.1
AW-C-dots 1.6 M	—	—	100.0	20.9	84.8
AW-C-dots 3.2 M	4.7	8.9	95.3	21.9	80.1

[a] A and τ correspond to the normalized amplitude and decay time constant, respectively. The systematic error is approximately ± 0.5 ns for all lifetime values.

emission can be obtained by eliminating the O-state and enhancing the N-state in the N-doped C-dots. The removal of O-state can reduce the recombination of surface defect states with a wide distribution of energy levels. This conclusion is further supported by the PL decay spectra in figure 4(f), which are detected at 439 nm (PL peak) with an excitation of 350 nm. All the curves are well fitted with a biexponential function, except for the AW-C-dots 1.6 M with a single exponential function. The best-fit parameters are listed in table 2, where the longer component (τ_2) is assigned to the radiative recombination of the electron-hole pairs and the shorter one is attributed to the defect centers of the C-dots. This table clearly shows that with the decrease of O-state, the ratio of the longer component becomes larger, leading to a higher PLQY.

The key role of AW on the structure and PLQY of C-dots is summarized in figure 1(b). For OR-C-dots, the high surface N-states are formed due to the effective passivation of amide groups, which facilitates the radiative recombination and leads to high PLQY, although there are still some O defect states induced by the O-containing functional groups. The use of moderate AW in reaction precursors helps to eliminate the O-state and enhance the N-state, and finally leads to an enhancement of PLQY from 76.7% (OR-C-dots) to 84.8% (AW-C-dots). However, excessive AW would block the removal of O-state, leading to fluorescence quenching to some extent, although at the same time N-state is enhanced. The above discussion could be a general way to achieve the highly luminescent C-dots: first, the proper N-containing reaction precursors (such as CA and EDA) should be chosen to realize excellent surface N-state, and then some reagents (like AW) should be used to effectively reduce oxygen inside the C-dots.

3.4. Application

The highly luminescent C-dots exhibit great potential applications in optoelectronic devices as an LDS material. For example, SiNW solar cells are one of the most ideal platforms for the application of the C-dots LDS layer; they possess excellent antireflection characteristics [40–42] but still have much poor EQE in the UV region [43, 44]. It is anticipated that the LDS layer can greatly enhance the EQE of the SiNW solar cells in the UV region, since the resultant highly luminescent C-dots effectively down-shift the photons in the UV region into photons with wavelengths of ~439 nm, where the EQE of the SiNW solar cells is much higher. We have employed PVA as the host material for the LDS layer due to its high transmittance and good compatibility with our yielded C-dots (since the PLQY of the close-packed C-dots can be dramatically decreased owing to the aggregation-caused fluorescence quenching [8], and the C-dots aqueous solutions should not be spread on the SiNW solar cells directly). The AW-C-dots 1.6 M aqueous solutions and the PVA aqueous solutions (5 wt%) are mixed with different volume ratios and the LDS layers are fabricated on the surface of the SiNW solar cells through a spin-coating method. Figure 5(a) displays a typical SEM image of the SiNW solar cells coated with the C-dots/PVA films, which indicates that the film is excellently embedded in the SiNWs. The corresponding schematic diagram of the SiNW solar cells structure with the LDS layer is shown in figure 5(b).

To obtain the optimum concentrations of the C-dots in PVA as the best LDS layer, we have carefully investigated the EQE of the SiNW solar cells coated with different LDS layers fabricated by varying the volume ratios of the C-dots solutions to PVA solutions (all the devices used are spin-coated five times), as shown in figure 5(c). Obviously, the EQE of the solar cells in the UV region gets the largest increase as the

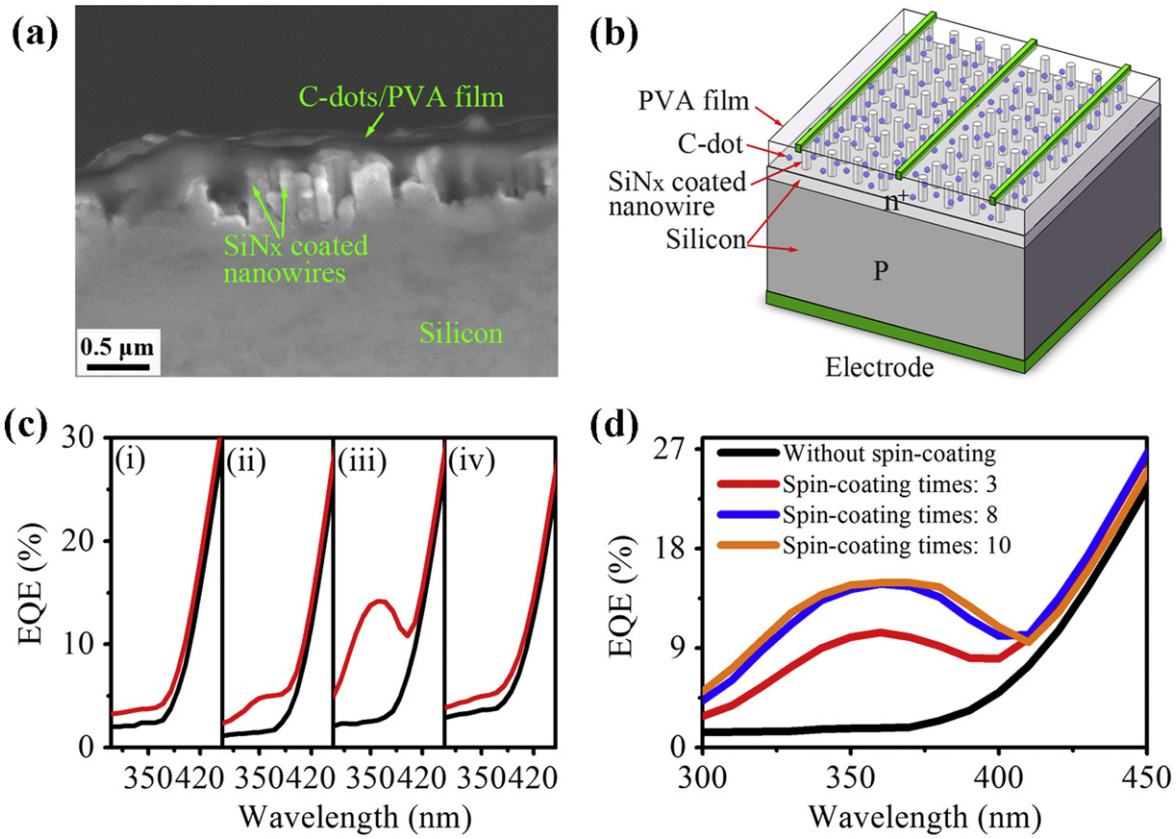

Figure 5. (a) SEM image and (b) Schematic diagram of SiNW solar cells coated with C-dots/PVA films. (c) EQE spectra of SiNW solar cells coated without (black curves) and with different volume ratios of the AW-C-dots 1.6 M doped PVA films (red curves): (i) 0%; (ii) 1.2%; (iii) 2.0%; (iv) 7.2% (spin-coating times are five). (d) EQE spectra of SiNW solar cells with different spin-coating times of PVA film with 2.0% volume ratio of the AW-C-dots 1.6 M.

volume ratio of the C-dots is 2.0%. When the volume ratio is lower than this, the amount of the C-dots in the LDS layer is insufficient, and, on the contrary, it will show some degree of the aggregation-caused fluorescence quenching, both of which can reduce the down-shifting efficiency. Meanwhile, we have also optimized the thickness of the LDS layer, embodied by spin-coating times. Figure 5(d) shows that the EQE enhancement in the UV region increases with the spin-coating times, but it hardly increases when the spin-coating times are more than eight. From the above observation, we can conclude that a volume ratio of 2.0% for the C-dots with spin-coating times of eight is the best production process for the LDS layer.

3.5. EQE spectra analysis

Figure 6(a) contrastively shows the EQE spectra of the SiNW solar cells coated with and without the LDS layer prepared under the optimal production process. The dotted boxes demonstrate three EQE-changing regions after the LDS layer coating: (i) LDS region; (ii) medium-wave band; and (iii) long-wave band. In the LDS region, the EQE enhancement profile is consistent with the C-dots absorption spectrum in the UV region, which confirms the contribution of the down-shifting effect to the EQE enhancement. The EQE changes in the medium- and long-wave bands are zoomed-in in figures 6(b) and (c), respectively, in order to better observe the influence of the LDS layer on the EQE in these two regions. The EQE is increased in the medium-wave band but decreased in the long-wave band after the LDS layer coating, and these features cannot simply be ascribed to photons down-shifting, since there is almost no absorption for the C-dots above 400 nm. In addition, the SiNWs are covered by a SiN_x layer, which effectively passivates the surface defect states and isolates the LDS layer from the SiNWs; hence the LDS layer hardly influences the electrical properties of the SiNW solar cells. We therefore attribute the EQE changes in the medium- as well as in the long-wave bands to the alteration of the optical properties of the devices.

To clarify the origin of the EQE changes, the reflectance spectra of the uncoated SiNW solar cells and cells with the LDS layer or the PVA film are measured, as shown in figure 6(d). In the UV region, the reflectance of the SiNW solar cells coated with the LDS layer is higher than that of the uncoated SiNW solar cells (resulting from the outward-running photons generated by the C-dots in the LDS layer, which is evidenced by comparing the reflectance spectrum of the SiNW solar cells coated with the pure PVA film). Above 400 nm, the reflectance of the SiNW solar cells coated with the LDS layer is slightly higher than that of the uncoated cells. For the LDS layer coated devices, the decreased EQE in the long-wave band (shown in figure 6(c)) should be caused

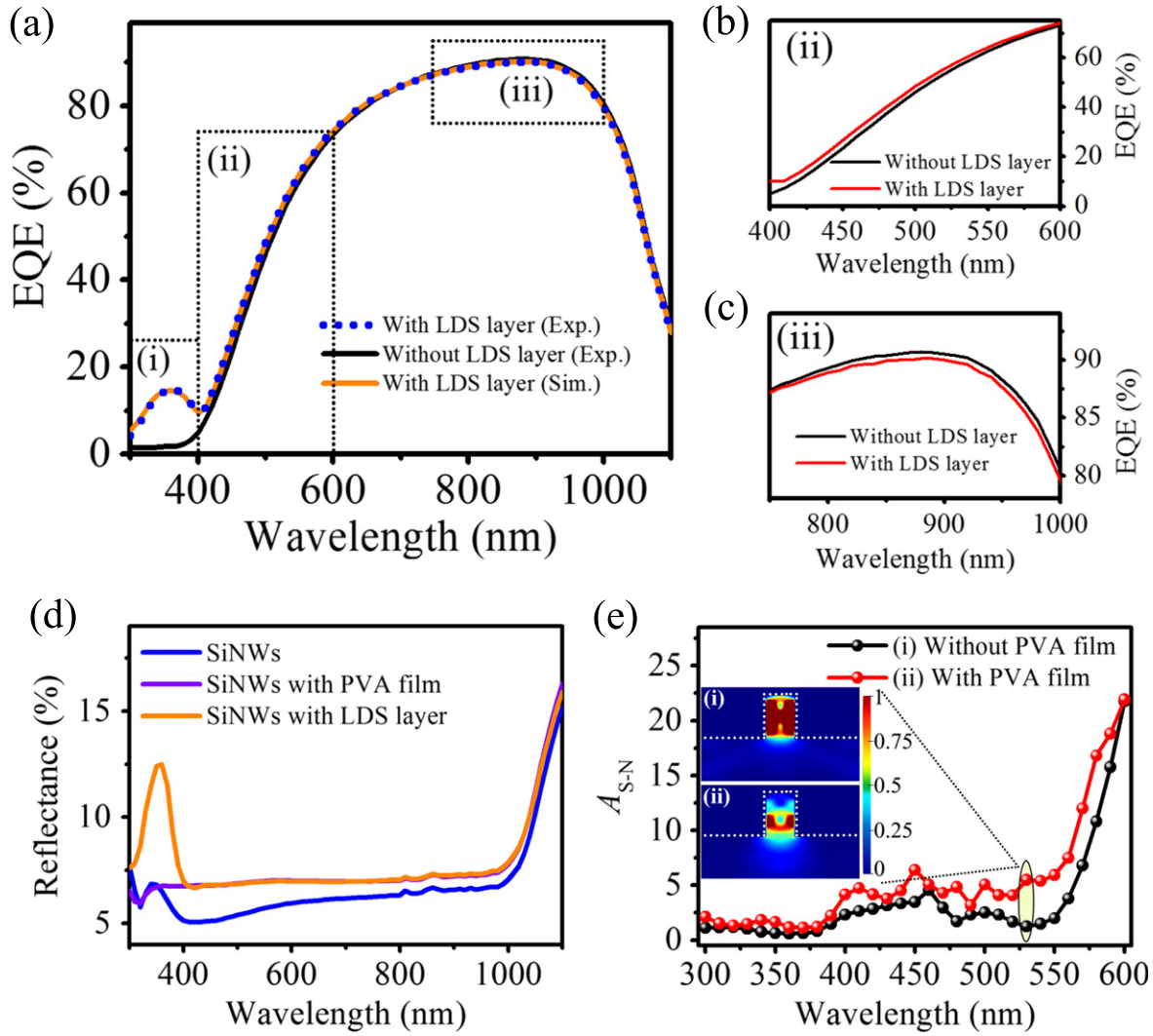

Figure 6. (a) EQE spectra of the SiNW solar cells coated with (blue dotted curve from experiment; orange solid curve from simulation) and without (black solid curve) an LDS layer. Amplified EQE spectra measured from experiment in (b) medium-wave band (ii) and (c) long-wave band (iii). (d) Reflectance spectra of SiNW solar cells uncoated (blue) and coated with PVA film (violet) and LDS layer (orange). (e) Dependence of the $A_{S\text{-}N}$ factor on the wavelengths for the SiNW solar cells with (red) and without (black) PVA film. Inset: the light absorption distribution profiles of the SiNW solar cells with and without PVA film under 530 nm illumination. The dotted white lines indicate the profiles of the SiNWs and the substrates, and the color scale is normalized.

by the increased reflectance property. However, the EQE in the medium-wave band is still enhanced, even though the reflectance gets worse, indicating the improved internal quantum efficiency (IQE). We note that this phenomenon can also be observed in the SiNW solar cells with pure PVA film, which suggests that this feature is mainly due to the PVA film rather than the luminescent C-dots. To explain the interesting enhancement of the IQE in the medium-wave band, we contrastively simulate the absorption spectra for the pure PVA film coated and uncoated SiNW solar cells by the finite difference time domain method. Figure 6(e) shows the dependence of the $A_{S\text{-}N}$ factor (the ratio of light absorption in silicon substrate to SiNWs) on the wavelengths. It is obvious that the $A_{S\text{-}N}$ values increase in the medium-wave band (400–600 nm) after coating the SiNW solar cells with PVA film, demonstrating the enhanced optical field in the substrate together with reduced optical field in the SiNWs, which is intuitively confirmed by the optical field distribution profiles (illuminated under $\lambda = 530$ nm), as shown in the inset of figure 6(e). As we know, there is severe carrier recombination in the SiNWs, which even acts as a 'dead layer' in terms of electric properties [28]—thus higher $A_{S\text{-}N}$ leading to higher IQE.

3.6. Extraction of the down-shifting contribution

We have calculated the increment of the short-circuit current density (ΔJ_{SC}) based on the EQE curves of the SiNW solar cells with and without the LDS layer under the AM 1.5G spectrum between 300 and 1100 nm to evaluate the benefits

of the LDS layer. The formula is presented as follows [1, 9]:

$$\Delta J_{SC} = q \int_{300\,\mathrm{nm}}^{1100\,\mathrm{nm}} \Phi(\lambda) \times \left[EQE_{coated}(\lambda) - EQE_{uncoated}(\lambda)\right] d\lambda \quad (1)$$

where q is the electron charge (1.6×10^{-19} C) and $\Phi(\lambda)$ is the incident photon flux of a given spectra (AM 1.5G). The ΔJ_{SC} is calculated to be as high as 0.30 mA cm^{-2} by using the EQE spectra measured from experiment, which originates from three aspects: down-shifting, reflectance and optical absorption redistribution. In order to extract quantitatively the contribution from the down-shifting part, we present a simple yet effective model to better understand the measured EQE spectrum of the solar cells with LDS layers:

$$EQE_{coated}(\lambda) = \frac{m_A(\lambda)}{n_0(\lambda)} + \frac{m_G(\lambda)}{n_0(\lambda)} \quad (2)$$

where n_0 is the number of incident photons, m_A and m_G are the photoelectrons generated by the original incident photons and the converted photons, respectively, and expressed as

$$m_A(\lambda) = [1 - R(\lambda)][1 - A(\lambda)] n_0(\lambda) \cdot IQE_{coated}(\lambda) \quad (3)$$

$$m_G(\lambda) = [1 - R(\lambda)] A(\lambda) \cdot \eta \cdot n_0(\lambda) \cdot PLQY \cdot \int_{\lambda_1}^{\lambda_2} EM(\lambda') \cdot IQE_{coated}(\lambda') d\lambda' \quad (4)$$

R and IQE_{coated} are the reflectance and IQE of the SiNW solar cells coated with pure PVA films, respectively, A is the fraction of incident light absorbed in the LDS layer, $EM(\lambda)$ is the normalized emission profile of the C-dots, λ_1 and λ_2 are the wavelengths of the two endpoints of the emission spectrum. The collection efficiency (η) factors losses induced by reabsorption and light emitted away from the solar cells.

This model is used to fit the measured EQE spectrum of the LDS layer coated SiNW solar cells, and a good fit for the EQE enhancement is obtained by varying the magnitude of the C-dots absorption and the collection efficiency, as shown in figure 6(a). It should be noticed that the collection efficiency used here is 68.0%, indicating that most of the isotropically emitted photons enter the devices. The ΔJ_{SC} from down-shifting ($\Delta J_{SC\text{-}DS}$) is calculated to be 0.13 mA cm^{-2} by equation (5) below, which makes up 43.3% of the J_{SC} enhancement; the rest (56.7%) should be attributed to the competing result of the reflectance and the optical absorption redistribution (owing to the great contribution from the optical field redistribution, an increase in J_{SC} can also be observed for the solar cells with a lower PLQY C-dots but with a smaller increment).

$$\Delta J_{SC-DS} = q \int_{300\,\mathrm{nm}}^{1100\,\mathrm{nm}} \Phi(\lambda) \left\{ m_G(\lambda)/n_0(\lambda) - [1 - R(\lambda)] A(\lambda) \cdot IQE_{coated}(\lambda) \right\} d\lambda \quad (5)$$

Finally, it is worth mentioning that the fluorescence is very stable, discerning from the EQE spectra of the LDS layer coated solar cells with different storage times (shown in figure S3). Furthermore, the photovoltaic current–voltage characteristics are measured at standard test conditions. The J_{SC} of the SiNW solar cells increases from 29.25 to 29.55 mA cm^{-2} and the ΔJ_{SC} is 0.30 mA cm^{-2}—a good agreement with the calculated ΔJ_{SC} from the EQE. Its power conversion efficiency increases from 10.85% to 10.96%, corresponding to a 0.11% absolute enhancement, with invariant open-circuit voltage (0.53 V) and fill-factor (70.0%). It should be noted that the power conversion efficiency of solar cells can be further improved by 1) widening the absorption band of C-dots in the region where the spectral response of the solar cells is poor and 2) making the emission band of C-dots coincide with the best spectral response region of solar cells, on the basis of a large Stokes shift and high PLQY of C-dots.

4. Conclusions

In summary, a new strategy for synthesizing highly luminescent C-dots has been proposed and thoroughly investigated. On the basis of successful realization of PLQY of 76.7% C-dots with CA as the carbon source and EDA as the nitrogen source, we have added moderate AW to the reaction precursors to achieve both appropriate inner structure and excellent N passivation. The effect of pH value and AW amount on the luminescence properties has been carefully examined and the PLQY of the resultant C-dots reaches as high as 84.8%, benefiting from the fact that the AW acts as not only the surface-passive agent, but also the inner N-doped O-containing structure modifier. An effective enhancement of J_{SC} has been observed when integrating the C-dots with the highest PLQY into PVA to form LDS layers on the SiNW solar cells. The underlying mechanism of the enhancement is attributed to the competing result of the deterioration of surface reflectance and the gains from the optical absorption redistribution as well as the down-shifting; the down-shifting contribution (43.3%) is accurately extracted by our proposed theoretical model. We believe that the high-performance, stable and low-toxic C-dots synthesized through our method are promising LDS materials applied to optoelectronic devices.

Acknowledgments

This work was supported by the National Natural Science Foundation of China (61234005, 11174202, 11304197 and 11474201).

References

[1] Liu J, Wang K, Zheng W, Huang W, Li C H and You X Z 2013 *Prog. Photovolt., Res. Appl.* **21** 668–75
[2] Le Donne A, Acciarri M, Narducci D, Marchionna S and Binetti S 2009 *Prog. Photovolt., Res. Appl.* **17** 519–25

[3] Sheng X, Corcoran C J, He J, Shen L, Kim S, Park J, Nuzzo R G and Rogers J A 2013 *Phys. Chem., Chem. Phys.* **15** 20434–7
[4] Hodgson S D, Brooks W S M, Clayton A J, Kartopu G, Barrioz V and Irvine S J C 2013 *Nano Energy* **2** 21–7
[5] Dai Prè M, Morrow I, Martin D J, Mos M, Del Negro A, Padovani S and Martucci A 2013 *Mater. Chem. Phys.* **139** 531–6
[6] Chen H C, Lin C C, Han H W, Tsai Y L, Chang C H, Wang H W, Tsai M A, Kuo H C and Yu P 2011 *Opt. Express* **19** A1141–7
[7] Lin C C, Chen H C, Tsai Y L, Han H V, Shih H S, Chang Y A, Kuo H C and Yu P 2012 *Optics Express* **20** A319–26
[8] Li Y, Li Z, Wang Y, Compaan A, Ren T and Dong W J 2013 *Energy Environ. Sci.* **6** 2907–11
[9] McIntosh K R, Lau G, Cotsell J N, Hanton K, Bätzner D L, Bettiol F and Richards B S 2009 *Prog. Photovolt. Res. Appl.* **17** 191–7
[10] Klampaftis E and Richards B S 2011 *Prog. Photovolt. Res. Appl.* **19** 345–51
[11] Ross D, Klampaftis E, Fritsche J, Bauer M and Richards B S 2012 *Sol. Energy Mater. Sol. Cells* **103** 11–6
[12] Fang Y, Guo S, Li D, Zhu C, Ren W, Dong S and Wang E 2011 *ACS Nano* **6** 400–9
[13] Zhou J, Yang Y and Zhang C Y 2013 *Chem.Commun.* **49** 8605–7
[14] Wang F, Pang S, Wang L, Li Q, Kreiter M and Liu C Y 2010 *Chem. Mater.* **22** 4528–30
[15] Chen B *et al* 2013 *Nanoscale* **5** 1967–71
[16] Wu Z L, Zhang P, Gao M X, Liu C F, Wang W, Leng F and Huang C Z 2013 *J. Mater. Chem.* B **1** 2868–73
[17] Liu Y, Liu C Y and Zhang Z Y 2012 *Appl. Surf. Sci.* **263** 481–5
[18] Dong Y, Wang R, Li H, Shao J, Chi Y, Lin X and Chen G 2012 *Carbon* **50** 2810–5
[19] Zhu S, Meng Q, Wang L, Zhang J, Song Y, Jin H, Zhang K, Sun H, Wang H and Yang B 2013 *Angew. Chem. Int. Ed. Engl.* **52** 3953–7
[20] Wang F, Xie Z, Zhang H, Liu C Y and Zhang Y G 2011 *Adv. Funct. Mater.* **21** 1027–31
[21] Liu S, Tian J, Wang L, Zhang Y, Qin X, Luo Y, Asiri A M, Al-Youbi A O and Sun X 2012 *Adv. Mater.* **24** 2037–41
[22] Yang S T *et al* 2009 *J. Phys. Chem.* C **113** 18110–4
[23] Baker S N and Baker G A 2010 *Angew. Chem., Int. Ed. Engl.* **49** 6726–44
[24] Anilkumar P, Wang X, Cao L, Sahu S, Liu J H, Wang P, Korch K, Tackett I K N, Parenzan A and Sun Y P 2011 *Nanoscale* **3** 2023–7
[25] Hu X, Cheng L, Wang N, Sun L, Wang W and Liu W 2014 *RSC Adv.* **4** 18818–26
[26] Guo Y, Wang Z, Shao H and Jiang X 2013 *Carbon* **52** 583–9
[27] Dong Y, Pang H, Yang H B, Guo C, Shao J, Chi Y, Li C M and Yu T 2013 *Angew. Chem., Int. Ed. Engl.* **52** 7800–4
[28] Lin X X, Hua X, Huang Z G and Shen W Z 2013 *Nanotechnology* **24** 235402–9
[29] Peng H and Travas-Sejdic J 2009 *Chem. Mater.* **21** 5563–5
[30] Zhai X, Zhang P, Liu C, Bai T, Li W, Dai L and Liu W 2012 *Chem. Comm.* **48** 7955–7
[31] Wen X, Yu P, Toh Y R, Hao X and Tang J 2013 *Adv. Opt. Mater.* **1** 173–8
[32] Cushing S K, Li M, Huang F and Wu N 2014 *ACS Nano* **8** 1002–13
[33] Vempati S and Uyar T 2014 *Phys. Chem. Chem. Phys.* **16** 21183–203
[34] Qian Z, Ma J, Shan X, Shao L, Zhou J, Chen J and Feng H 2013 *RSC Adv.* **3** 14571–9
[35] Kumar G S, Roy R, Sen D, Ghorai U K, Thapa R, Mazumder N, Saha S and Chattopadhyay K K 2014 *Nanoscale* **6** 3384–91
[36] Wang L *et al* 2014 *ACS Nano* **8** 2541–7
[37] Eda G, Lin Y Y, Mattevi C, Yamaguchi H, Chen H A, Chen I S, Chen C W and Chhowalla M 2010 *Adv. Mater.* **22** 505–9
[38] Ma Z, Ming H, Huang H, Liu Y and Kang Z 2012 *New J. Chem.* **36** 861–4
[39] Liu C, Zhang P, Tian F, Li W, Li F and Liu W 2011 *J. Mater. Chem.* **21** 13163–7
[40] Shen X, Sun B, Liu D and Lee S T 2011 *J. Am. Chem. Soc.* **133** 19408–15
[41] Fute Z, Tao S and Baoquan S 2012 *Nanotechnology* **23** 194006–14
[42] Zhang F, Liu D, Zhang Y, Wei H, Song T and Sun B 2013 *ACS Appl. Mater. Interf.* **5** 4678–84
[43] Oh J, Yuan H C and Branz H M 2012 *Nat. Nanotechnology* **7** 743–8
[44] Huang B R, Yang Y K, Lin T C and Yang W L 2012 *Sol. Energy Mater. Sol. Cells* **98** 357–62